PERGAMON

International Journal of Solids and Structures 38 (2001) 4375–4394

INTERNATIONAL JOURNAL OF SOLIDS and STRUCTURES

www.elsevier.com/locate/ijsolstr

The effect of corner angles in bimaterial structures

Ilyas Mohammed, Kenneth M. Liechti *

Research Center for Mechanics of Solids, Structures and Materials, University of Texas at Austin, Austin, TX 78712-1085, USA

Received 2 August 1999; in revised form 5 October 2000

Abstract

The effect of the corner angle on bimaterial corner stresses is studied. Corners (with one side bonded) and joints (with both sides bonded) are studied considering the materials to be elastic and plastic. Two structures with bimaterial corners, lap and scarf joints are considered. For the elastic analysis, the singularity at the corner as well as the stress intensity factor are found for a range of angles using the Betti's law based reciprocal work contour integral theorem which combines the ease of finite element calculations far away from the corner with the singular representation near the corner. The singularity and the stress intensity factors were found to depend on the angle. For the work-hardening plastic analysis, a fourth order differential equation was solved to obtain the singularity at the corner and finite element solutions were used to obtain stress intensity factors. These parameters were found to depend on load level, hardening exponent and the angle. It is concluded that the stress intensity factors are unsuitable as failure criteria for a corner with varying angle. One exception was found to be for a corner with high yielding that gave rise to a constant stress intensity factor for different corner angles.

Keywords: Corner singularities; Elastoplastic; Stress intensity factors

1. Introduction

Due to the increasing use of adhesively bonded joints in aerospace and automotive industries and multiple layers in microelectronics packaging, many researchers have addressed the problem of stress singularities near bimaterial corners and joints. Williams (1952) showed that a stress singularity of type $r^{-\lambda}$ exists near a bimaterial corner where λ can be a complex number and $0 < \text{real}\ (\lambda) < 0.5$. Bogy (1971) calculated the real components of λ for different material properties and corner angles. Hein and Erdogan (1971) did the same and found the complex values of λ, both singular and non-singular ones. Carpenter and Byers (1987) calculated the stress intensity factor based on the technique developed by Stern et al. (1976). A singularity analysis based on the J_2 deformation theory was developed by Lau and Delale (1988) for corners and by Duva (1988) for joints. Reedy (1993) obtained the stress intensity factors for butt joints using the above theory.

* Corresponding author. Fax: +1-512-471-5500.
E-mail address: kml@mail.utexas.edu (K.M. Liechti).

0020-7683/01/$ - see front matter
PII: S0020-7683(00)00389-9

The study of angle variation in the bimaterial corners has received less attention. Many researchers such as Gradin (1982), Groth and Brottare (1988), Reedy and Guess (1993), Hattori et al. (1989) and Fernlund et al. (1994) have used stress intensity factors as nucleation criteria. These criteria have served well for bimaterial corners with the same corner angle. Some researchers (Hattori et al., 1989) have used stress intensity factors as nucleation criteria for varying corner angles (varying λ). For this criterion to work for varying corner angles, the stress intensity factor has to be able to capture the severity of the corner and should have a simple relationship with the corner angle. For instance, if the stress singularity decreases with increasing corner angle, the stress intensity factor and the corresponding stress near the corner should have a similar variation. If that is indeed the case, the stress intensity factor represents the severity of the corner and hence can be used as nucleation criterion.

In this study, the feasibility of using a stress intensity factor approach for establishing the severity of a variety of corners was examined. This was accomplished by considering lap and scarf joints where

1. The ratio of elastic moduli was varied.
2. The nature of the corner was changed (one side bonded vs. both sides bonded).
3. The corner angle was varied.

The joints were analyzed considering elastic and elastoplastic behavior. In the elastoplastic case, the effect of hardening exponent was also examined. The joints considered here contained no adhesive interlayers and will not be able to account for any thickness effects, should they arise.

2. Theory

2.1. Analysis for elastic materials

For an elastic material, the displacements and stresses can be expressed using complex potentials (Muskhelishvili, 1963)

$$\begin{aligned} U_m &= u_{mr} + \mathrm{i}u_{m\theta} = \left(\frac{1+\nu_m}{E_m}\right)\mathrm{e}^{-\mathrm{i}\theta}\left(\kappa_m\Omega_m(z) - z\bar{\Omega}'_m(\bar{z}) - \bar{\Psi}_m(\bar{z})\right) \\ \Sigma_{mr} &= \sigma_{mrr} + \mathrm{i}\sigma_{mr\theta} = \Omega'_m(z) + \bar{\Omega}'_m(\bar{z}) - \bar{z}\bar{\Omega}''_m(\bar{z}) - \frac{\bar{z}}{z}\bar{\Psi}'_m(\bar{z}) \\ \Sigma_{m\theta} &= \sigma_{m\theta\theta r} - \mathrm{i}\sigma_{mr\theta} = \Omega'_m(z) + \bar{\Omega}'_m(\bar{z}) + \bar{z}\bar{\Omega}''_m(\bar{z}) + \frac{\bar{z}}{z}\bar{\Psi}'_m(\bar{z}) \end{aligned} \tag{1}$$

where the subscript m corresponds to the material $m = 1$ or $m = 2$. Following the method of Stern et al. (1976), the complex potentials are assumed to be

$$\begin{aligned} \Omega_m(z) &= A_m z^{1-\lambda} + a_m z^{1-\bar{\lambda}} \\ \Psi_m(z) &= B_m z^{1-\lambda} + b_m z^{1-\bar{\lambda}} \end{aligned} \tag{2}$$

The solution procedure is the same as the one followed by Carpenter and Byers (1987). Substituting Eq. (2) in Eq. (1), and applying the following boundary conditions for the bimaterial corner shown in Fig. 1(a),

$$\begin{aligned} &U_1(\theta = 0) = U_2(\theta = 0) \\ &\Sigma_{1\theta}(\theta = 0) = \Sigma_{2\theta}(\theta = 0) \\ &\Sigma_{1\theta}(\theta = -\theta_1) = 0 \\ &\Sigma_{2\theta}(\theta = \theta_2) = 0 \end{aligned} \tag{3}$$

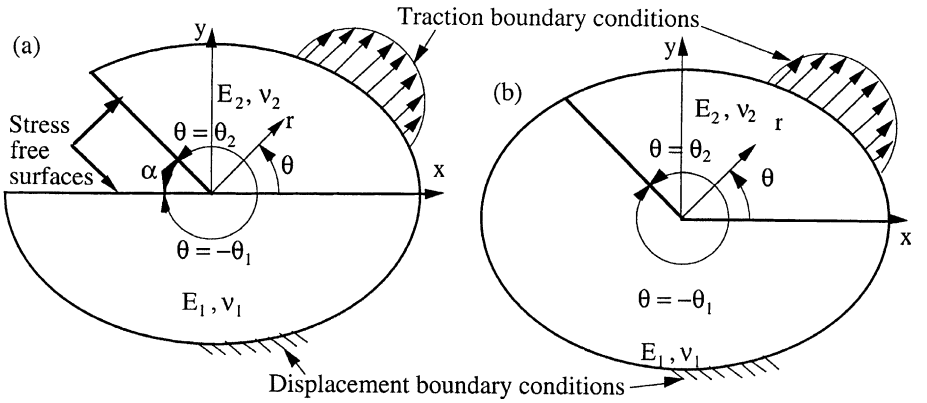

Fig. 1. (a) A bimaterial corner with only one interface bonded and (b) a bimaterial joint with both interfaces bonded.

yield a system of equations, which may be written as

$$[D]\{A_1 \quad A_2 \quad a_1 \quad a_2 \quad B_1 \quad B_2 \quad b_1 \quad b_2\}^{\mathrm{T}} = \{0\} \tag{4}$$

where, $D_{ij} = D_{ij}(E_1, E_2, v, v_2, \theta_1, \theta_2; \lambda)$.

The eigenvalues of the matrix D are the stress singularities at the corner. Similarly, for the joint shown in Fig. 1(b) where both the sides are bonded, the boundary conditions are,

$$\begin{aligned} &U_1(\theta = 0) = U_2(\theta = 0) \\ &\Sigma_{1\theta}(\theta = 0) = \Sigma_{2\theta}(\theta = 0) \\ &U_1(\theta = -\theta_1) = U_2(\theta = \theta_2) \\ &\Sigma_{1\theta}(\theta = -\theta_1) = \Sigma_{2\theta}(\theta = \theta_2) \end{aligned} \tag{5}$$

These boundary conditions yield another matrix similar to matrix D whose eigenvalues are the stress singularities for the joint. Once the stress singularities are known, the stresses are given as,

$$\sigma_{ij}(r, \theta) = \sum_{n=1}^{N} K^n r^{\mathrm{Re}(\lambda_n)} f_{ijn}\left(\mathrm{Re}(\lambda_n), \mathrm{Im}(\lambda_n), \frac{r}{L}, \theta\right), \tag{6}$$

where L is some characteristic length. Yang and Munz (1995) have given these stresses in more detail. As the emphasis in this study is the variation of bimaterial corner angles (θ_1, θ_2), the nature of the joint (single side and both sides bonded), the ratio of moduli, and the extraction of stress intensity factors using FEM, the emphasis is not on including many stress singularities but trying to determine the dominant one and its range of dominance. With this in mind, and considering the most dominant singularity, the normal and shear stress intensity factors can be written as

$$\begin{aligned} K_{\mathrm{I}} &= \frac{r^{-\mathrm{Re}(\lambda)} \sigma_{\theta\theta}(r, \theta = 0)}{f_{\theta\theta}\left(\mathrm{Re}(\lambda), \mathrm{Im}(\lambda), \frac{r}{L}, \theta = 0\right)} \\ K_{\mathrm{II}} &= \frac{r^{-\mathrm{Re}(\lambda)} \sigma_{r\theta}(r, \theta = 0)}{f_{r\theta}\left(\mathrm{Re}(\lambda), \mathrm{Im}(\lambda), \frac{r}{L}, \theta = 0\right)} \end{aligned} \tag{7}$$

Please note that K_{I} and K_{II} as given in Eq. (7) are derived from the same stress intensity factor, $K^n(n = 1)$. The stress intensity factors are non-dimensionalized as given below

$$K_{\mathrm{I}}^{*} = \frac{K_{\mathrm{I}} L^{\mathrm{Re}(\lambda)}}{\sigma_0}$$
$$K_{\mathrm{II}}^{*} = \frac{K_{\mathrm{II}} L^{\mathrm{Re}(\lambda)}}{\sigma_0} \tag{8}$$

This definition was chosen for the normal and shear stress intensity factors (K_{I} and K_{II}) to determine if a simple correlation exists between them and the corresponding stresses that can be expressed as a function of the corner angle and stiffness ratios of the two materials. This would greatly help in characterizing bimaterial joints of arbitrary angles and material properties with only a few experiments and finite element analyses. Otherwise, extensive experiments and analyses need to be carried out in order to obtain an empirical nucleation criterion that will be valid for all corner angles and stiffness ratios.

K_{I} and K_{II} given in Eq. (7) can be found using the reciprocal work contour integral theorem (RWCIM) developed by Stern et al. (1976). This method is based on Betti's law where the singular solutions are used near the corner and finite element solutions are used far away from the corner.

2.2. Analysis for J_2 deformation plastic materials

For the plasticity analysis, the material 1 is assumed to be rigid and the material 2 is assumed to follow the constitutive equations given in Eq. (7). Since the Airy stress function is assumed to be in variable separable form, it is not possible to assume that each materials is a different Ramberg–Osgood material unless it is also assumed that the hardening exponents are the same (Lau and Delale, 1988). The assumption of one material being rigid and the other material being a Ramberg–Osgood material is reasonable since the bimaterials are usually made of materials with at least one order of magnitude difference in the stiffness. This is certainly the case for polymer based composites, encapsulation of chips, adhesives, joints, etc.

Near the corner, the elastic strains are negligible compared to the plastic strains and hence can be neglected. The strains are then given by

$$\varepsilon_{ij} = \frac{3}{2}\frac{\alpha}{E}\left(\frac{\sigma_{\mathrm{e}}}{\sigma_{\mathrm{Y}}}\right)^{n-1} S_{ij} \tag{9}$$

For plane strain conditions, these strains reduce to

$$\varepsilon_{rr} = \frac{3}{2}\frac{\alpha}{E}\left(\frac{\sigma_{\mathrm{e}}}{\sigma_{\mathrm{Y}}}\right)^{n-1}(\sigma_{rr} - \sigma_{\theta\theta})$$
$$\varepsilon_{\theta\theta} = \frac{3}{2}\frac{\alpha}{E}\left(\frac{\sigma_{\mathrm{e}}}{\sigma_{\mathrm{Y}}}\right)^{n-1}(\sigma_{\theta\theta} - \sigma_{rr}) \tag{10}$$
$$\varepsilon_{r\theta} = \frac{3}{2}\frac{\alpha}{E}\left(\frac{\sigma_{\mathrm{e}}}{\sigma_{\mathrm{Y}}}\right)^{n-1}\sigma_{r\theta}$$

where,

$$\sigma_{\mathrm{e}} = \left(\tfrac{3}{2}S_{ij}S_{ij}\right)^{1/2} = \left(\tfrac{3}{4}(\sigma_{rr} - \sigma_{\theta\theta})^2 + 3\sigma_{r\theta}^2\right)^{1/2}$$

Assuming the Airy stress function to be in variable separable form, let

$$\phi = r^{-\lambda+2}F(\theta)$$

The stresses reduce to

$$\begin{aligned}\sigma_{rr} &= r^{-\lambda}\left[F''(\theta) + (-\lambda+2)F(\theta)\right]\\ \sigma_{\theta\theta} &= r^{-\lambda}[(-\lambda+2)(-\lambda+1)F(\theta)]\\ \sigma_{r\theta} &= r^{-\lambda}\left[-(-\lambda+1)F'(\theta)\right]\end{aligned} \tag{11}$$

where, $(\ )' \equiv \partial/\partial\theta(\ )$.

The strains can be found using the plane strain constitutive equations (Eq. (8)). The displacements then follow from the strain displacement equations.

$$\varepsilon_{rr} = \frac{\partial u_r}{\partial r} \Rightarrow u_r = \frac{3}{4}\frac{\alpha}{E}\frac{1}{\sigma_Y^{n-1}}\frac{r^{-\lambda n+1}}{-\lambda n+1}(g(\lambda,\theta))^{n-1}f(\lambda,\theta) \tag{12}$$

$$\begin{aligned}\varepsilon_{r\theta} &= \frac{1}{2}\left[\frac{1}{r}\frac{\partial u_r}{\partial\theta} + \frac{\partial u_\theta}{\partial r} - \frac{u_\theta}{r}\right] \Rightarrow \frac{\partial}{\partial r}\left(\frac{u_\theta}{r}\right) = \frac{2}{r}\varepsilon_{r\theta} - \frac{1}{r^2}\frac{\partial u_r}{\partial\theta}\\ u_\theta &= \frac{3}{2}\frac{\alpha}{E}\frac{1}{\sigma_Y^{n-1}}\frac{r^{-\lambda n+1}}{\lambda n}\left[2g^{n-1}(-\lambda+1)F' + \frac{1}{2(1-\lambda n)}\left\{g^{n-1}\frac{\partial f}{\partial\theta} + (n-1)g^{n-2}\frac{\partial g}{\partial\theta}f\right\}\right]\end{aligned} \tag{13}$$

where,

$$g(\lambda,\theta) = \sqrt{\left[\frac{3}{4}(F''(\theta) + \lambda(-\lambda+2)F(\theta))^2 + 3(-(-\lambda+1)F'(\theta))^2\right]} \tag{14}$$

and

$$f(\lambda,\theta) = F''(\theta) + \lambda(-\lambda+2)F(\theta) \tag{15}$$

Assuming material 1 to be rigid in Fig. 1(a), the boundary conditions reduce to

$$\begin{aligned}&\sigma_{\theta\theta}(\theta=\theta_2) = 0 \Rightarrow F(\theta_2) = 0\\ &\sigma_{r\theta}(\theta=\theta_2) = 0 \Rightarrow F'(\theta_2) = 0\\ &u_r(\theta=0) = 0 \Rightarrow F''(0) + \lambda(-\lambda+2)F(0)\\ &u_\theta(\theta=0) = 0 \Rightarrow F'''(0) + F'(0)[4(1-\lambda n)(-\lambda+1) + \lambda(-\lambda+2)] = 0\end{aligned} \tag{16}$$

Finally, using the compatibility equation,

$$\frac{\partial^2\varepsilon_{\theta\theta}}{\partial r^2} + \frac{1}{r^2}\frac{\partial^2\varepsilon_{rr}}{\partial\theta^2} + \frac{2}{r}\frac{\partial\varepsilon_{\theta\theta}}{\partial r} - \frac{1}{r}\frac{\partial\varepsilon_{rr}}{\partial r} = 2\left[\frac{\partial^2\varepsilon_{r\theta}}{\partial r\partial\theta} + \frac{1}{r^2}\frac{\partial\varepsilon_{r\theta}}{\partial\theta}\right]$$

yields the fourth order governing differential equation,

$$\frac{\partial^4 F}{\partial\theta^4} = \frac{h(\lambda,\theta,n)}{H(\lambda,\theta,n)} - \lambda(-\lambda+2)F'' \tag{17}$$

where

$$\begin{aligned}h(\lambda,\theta,n) = {} & \lambda n(\lambda n-2)g^{n-1}f - 4(-\lambda n+1)(-\lambda+1)\left[(n-1)g^{n-2}\frac{\partial g}{\partial\theta}F' + g^{n-1}F''\right] - 2(n-1)g^{n-2}\frac{\partial g}{\partial\theta}\frac{\partial f}{\partial\theta}\\ & - (n-1)(n-2)g^{n-3}\left(\frac{\partial g}{\partial\theta}\right)^2 f + (n-1)g^{n-5}f\left(\frac{1}{4}\left[\frac{3}{2}f\frac{\partial f}{\partial\theta} + 6(-\lambda+1)^2F'F''\right]^2\right)\\ & - (n-1)g^{n-3}f\left(\frac{1}{2}\left[\frac{3}{2}\left(\frac{\partial f}{\partial\theta}\right)^2 + 6(-\lambda+1)^2\left((F'')^2 + F'F''''\right)\right]\right)\end{aligned}$$

and $H(\lambda,\theta,n) = g^{n-1} + \frac{3}{4}(n-1)g^{n-3}(f)^2$ where the functions g and f are defined in Eqs. (12) and (13) respectively. Hence, a homogeneous fourth order differential equation (Eq. (13)) with four homogeneous boundary conditions (Eq. (12)) is obtained. As this equation is highly non-linear, only a numerical solution is possible. As this is an eigenvalue problem, let

$$F(0) = 1 \tag{18}$$

without loss of generality. This makes the boundary conditions and hence the solution a unique one. The solution strategy is to guess the value of the singularity, λ such that assumption (Eq. (16)) is satisfied. For the case of the joint (Fig. 1(b)) where both the sides of the corner are bonded, the boundary conditions become,

$$\begin{aligned}
&u_r(\theta=0) = 0 \Rightarrow F''(0) + \lambda(-\lambda+2)F(0)\\
&u_\theta(\theta=0) = 0 \Rightarrow F'''(0) + F'(0)[4(1-\lambda n)(-\lambda+1) + \lambda(-\lambda+2)] = 0\\
&u_r(\theta=\theta_2) = 0 \Rightarrow F''(\theta_2) + \lambda(-\lambda+2)F(\theta_2)\\
&u_\theta(\theta=\theta_2) = 0 \Rightarrow F'''(\theta_2) + F'(\theta_2)[4(1-\lambda n)(-\lambda+1) + \lambda(-\lambda+2)] = 0
\end{aligned}$$

As mentioned by Duva (1988), two parameters λ and say, $F(\theta_2)$ have to be guessed and this complicates the problem with the resulting non-convergence to the solution. One way to avoid this problem is to note that the problem is symmetric about $\theta = \theta_2/2$ and solve the problem only over half the domain. The last two boundary conditions can be replaced by,

$$\begin{aligned}
&\sigma_{r\theta}\left(\theta = \frac{\theta_2}{2}\right) = 0 \Rightarrow F'\left(\frac{\theta_2}{2}\right) = 0\\
&u_\theta\left(\theta = \frac{\theta_2}{2}\right) = 0 \Rightarrow F'''\left(\frac{\theta_2}{2}\right) + F'\left(\frac{\theta_2}{2}\right)[4(1-\lambda n)(-\lambda+1) + \lambda(-\lambda+2)] = 0
\end{aligned}$$

Now, only one parameter, λ needs to be guessed as in the previous case (corresponding to the boundary conditions in Eq. (14). Runge–Kutta with multiple shooting method was used for both the problems. To find the stress intensity factors, a finite element analysis with a very fine mesh was used. The region of K dominance was found and the stress intensity factor extracted from the stresses along the interface.

3. Results and discussion

3.1. Elasticity solution

Bogy (1971) and Hein and Erdogan (1971) have given the real and complex stress singularities for a variety of material properties and corner angles. In this paper, as the emphasis is on studying the angular dependence of the properties of the corner and joint, two bimaterial structures shown in Figs. 2(a) and 3(a) were chosen. The material properties are $E_1 = 69$ GPa, $\nu_1 = 0.3$, $\nu_2 = 0.4$, and for the bimaterial corner A in Fig. 2(a), $\theta_1 = -180°$, and θ_2 and E_2 were varied. For corner B, $\theta_2 = -180°$, and θ_1 and E_2 were varied. These values were substituted in the D matrix given in Eq. (4) and the eigenvalues were found by equating the determinant of the matrix D to zero. This yields a series of eigenvalues for each set of the chosen variables. For the displacements and the strain energy to be bounded, the eigenvalues must satisfy the condition, $\mathrm{Re}\,(\lambda) < 0.5$. This range of eigenvalues also includes those that do not give rise to stress singularities. However in Figs. 4 and 5, only the strongest singularity is plotted for varying angles and stiffness ratios, $\rho = E_2/E_1$.

As shown in Fig. 4, the singularity generally increases with θ_2 except for a slight decrease where the singularity becomes complex. This point changes with the ratio, ρ and is nearly 180° for $\rho = 0.5$, as can be

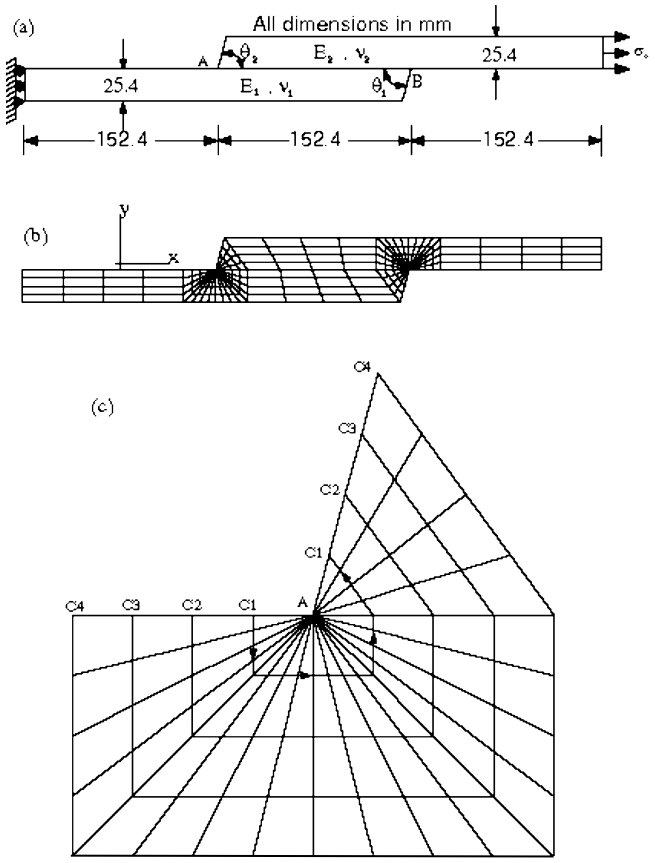

Fig. 2. (a) The lap joint, (b) the finite element discretization, and (c) the contours near the corner A.

seen from the plot. This is also the point where a weaker singularity becomes identical to the dominant one. As the stiffness of material 2 decreases, the singularity decreases. For small material 2 stiffness, there is practically no singularity for $\theta_2 < 45°$. For corner B, the stress singularity is plotted in Fig. 5 and is very strong for practically all angles except when the stiffness of material 2 is very close to that of the material 1. Hence, dependence of the singularity on the stiffness ratio for corner A is opposite to that of corner B.

To obtain the stress intensity factors, use was made of the RWCIM of Stern et al. (1976) and explained in detail by Carpenter and Byers (1987). As mentioned previously, this method is based on Betti's law where the singular solutions are used near the corner and finite element solutions are used far away from the corner. As the finite element solution is only needed far away from the corner, a coarse mesh is sufficient, thereby reducing computational costs and minimizing dependence on numerical accuracy of the solution.

Figs. 2(b) and 3(b) show the finite element discretization for the bimaterial structures shown in Figs. 2(a) and 3(a) respectively. The mesh near the corners A and C are shown in Figs. 2(c) and 3(c) respectively. Each element has a side of size $h/4$ in Fig. 2(c) and $h/8$ in Fig. 3(c), where h is the height of the specimen. The four contours, C1–C4 considered for integration are also shown. Using these four contours, the stress intensity factors and hence the stresses and displacements near the corner can be found. To begin with, the first four stress singularities were used to obtain the stresses near the corner. The effect of including more than one stress singularity is considered later. To verify the accuracy, the stresses found by this method were compared with the stress values obtained using finite element analysis with a very fine mesh near the corner.

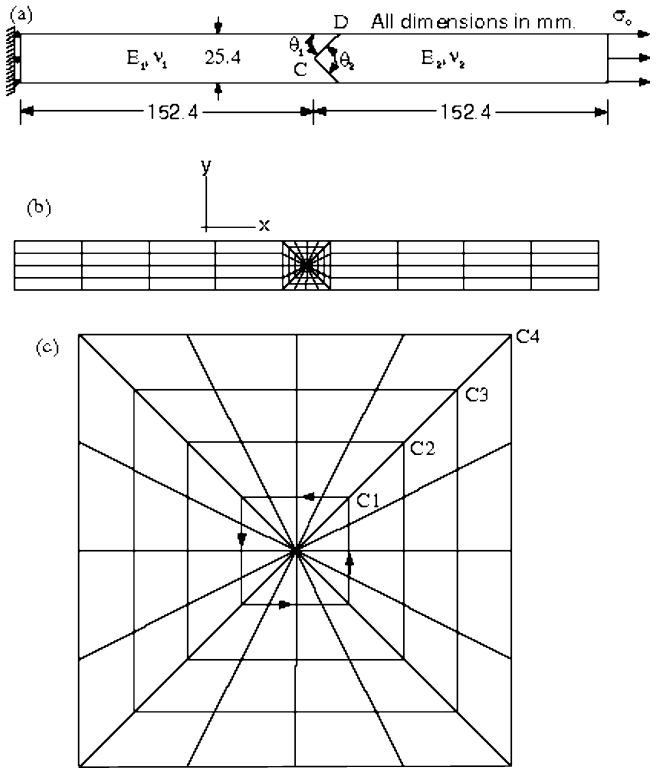

Fig. 3. (a) The scarf joint, (b) the finite element discretization, and (c) the contours near the corner C.

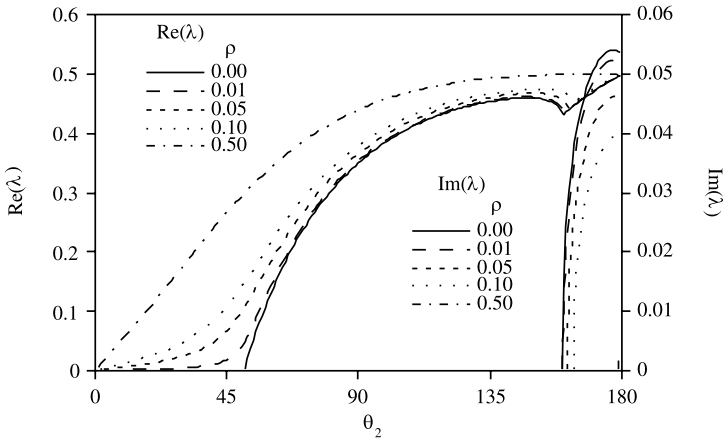

Fig. 4. Stress singularity at corner A in Fig. 2(a).

To verify the suitability of the chosen mesh near the corner, the normalized normal stress, $\sigma_{\theta\theta}/\sigma_0$ and shear stress, $\sigma_{r\theta}/\sigma_0$ along the interface were plotted over 10 decades in r/h in Figs. 6(a) and (b). The stresses were normalized by dividing by the applied stress, σ_0. The following values were chosen; $E_1 = 69$ GPa,

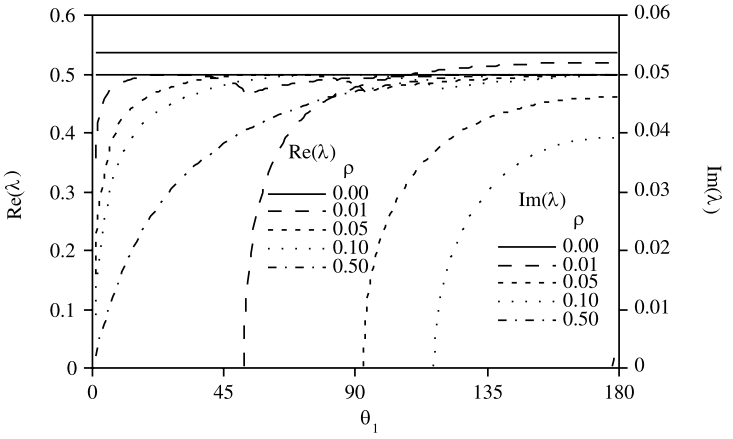

Fig. 5. Stress singularity at the corner B in Fig. 2(a).

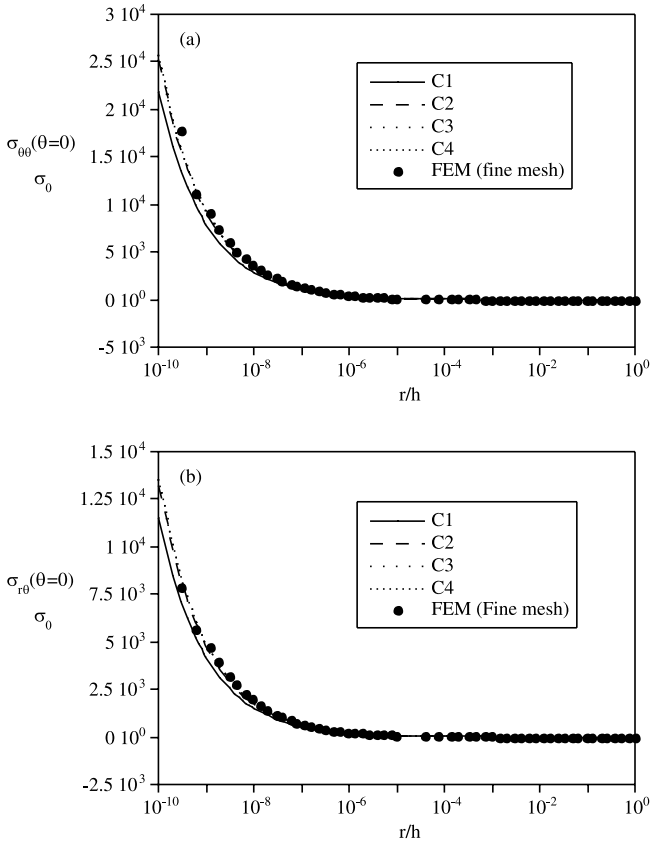

Fig. 6. Comparison of solutions using RWCIM and FEM for corner A.

$v_1 = 0.3$, $v_2 = 0.4$, $\rho = 0.5$, $\theta_1 = -180°$, and $\theta_2 = 90°$. The finite elements solution obtained using a very fine mesh was also plotted. As can be seen from these plots, except for contour C1, all other contour values

agree very well with the finite elements solution. This shows that the chosen mesh is adequate and gives excellent results near the corner.

The effect of using more that one stress singularity (eigenvalue) was also considered. The first four stress singularities for the choice of parameters given above are; $\lambda_1 = 0.4395$, $\lambda_2 = 0.0382$, $\lambda_3 = -0.7481 + i0.3808$, and $\lambda_4 = -1.068 + i0.2714$. Hence there are two singular and two non-singular eigenvalues for this set of parameters. The normalized normal and shear stresses along the interface are plotted in Fig. 7(a) and (b) where N is the number of stress singularities used for the calculation of the stresses. The shear stresses are in good agreement with the finite elements solution over the range $10^{-10} < r/h < 10^{-2}$ for all values of N. The normal stress for $N > 1$ agrees very well with the finite elements solution. The $N = 1$ curve deviates from the rest of the curves.

As these plots are made using a logarithmic scale, the slope of the lines near the corner should give the dominant singularity. This is indeed the case as the slope of both the lines is in excellent agreement with the λ_1 value. This also shows that there is a region near the corner where the stress singularity dominates. By considering the two plots, this region is $r/h < 10^{-5}$.

To look into the effect of N further from the corner, the above stresses were plotted over the range $10^{-2} < r/h < 1$ as shown in Fig. 8(a) and (b). From the normal stress curves, it is seen that $N = 2$ is the correct choice. From the shear stress curves, it is seen that the finite element solution is close to the two curves $N = 1$ and $N = 2$. Hence, further from the corner, the first two stress singularities should be used to

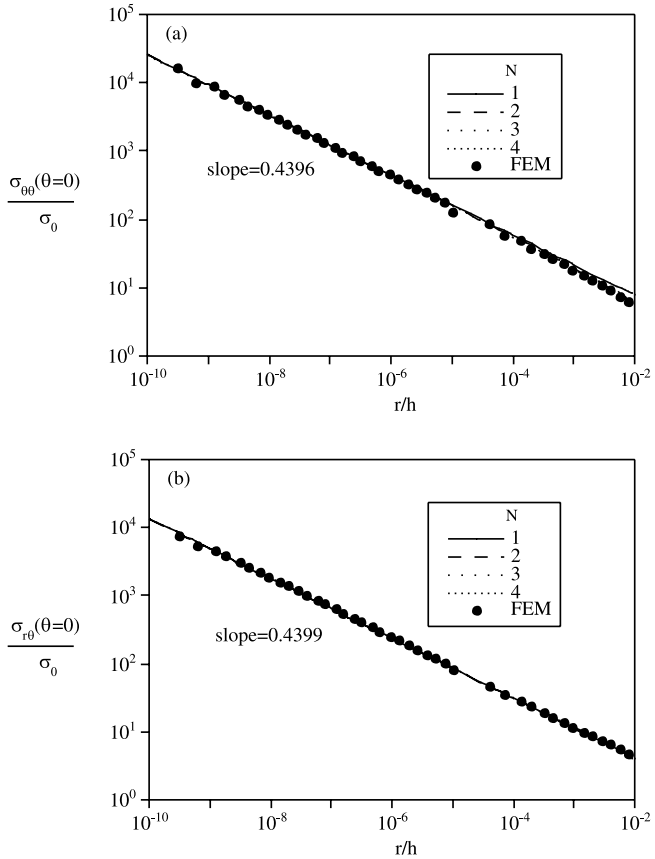

Fig. 7. The elastic singularity zone at corner A.

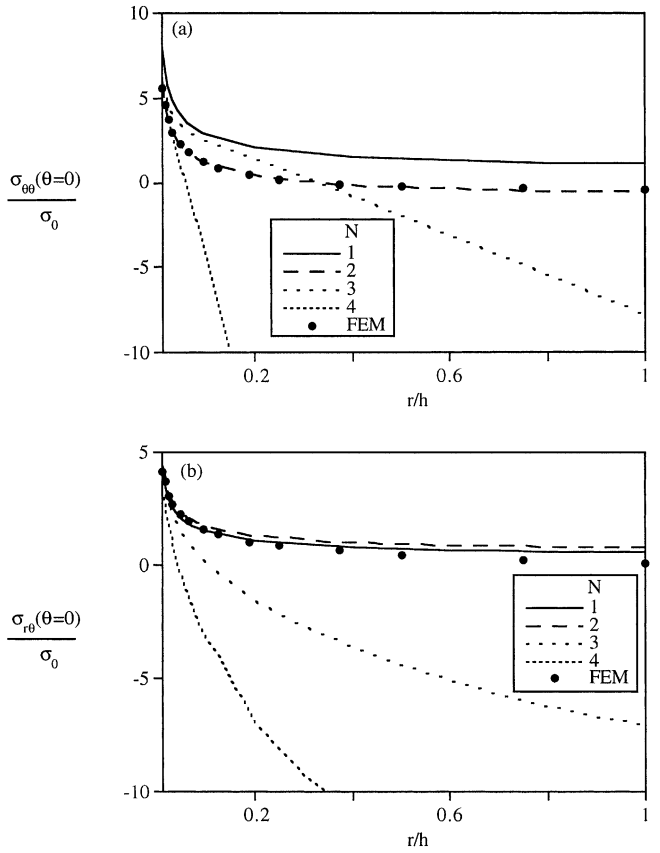

Fig. 8. The effect of the number of stress singularities (N) on the stresses.

obtain the stresses and displacements. The stress values when the two complex stress singularities are included seem to diverge over this range. Even though the reason for this divergence was not studied, it seems that the complex singularities are very sensitive to the boundary conditions and hence diverge from the solution for large values of r/h. Hence, it is shown from this study that there is a zone dominated by stress singularity and by using more than one stress singularity, the domain of convergence was found to be over eight decades. The results obtained using RWCIM were excellent over this range.

The normal and tangential stresses along the interface at corner A (lap joint, Fig. 2a) were calculated and plotted in Fig. 9(a) and (b). These values correspond to $r/h = 10^{-10}$. As can be seen from these figures, the stresses increase with increasing θ_2 and increasing value of stiffness ratio, ρ. The normalized stress intensity factors as given in Eq. (6) were plotted in Fig. 10(a) and (b). In general, the stress intensity factors increased for increasing values of ρ but decreased with increasing θ_2. Even though the stresses increased monotonically with ρ and θ_2, the stress intensity factors were not monotonic with respect to either parameter. This shows that the stress intensity factors, by themselves, are not in correspondence with the stresses in the same way as they are for cracks.

The same analysis was carried out for corner B. The normal and tangential stresses along the interface at corner B were calculated and plotted in Fig. 11(a) and (b). These stresses were evaluated at $r/h = 10^{-10}$. The stresses were not as regular as in the case of corner A. The non-monotonic nature of the stresses may be explained by the non-monotonic nature of the stress singularities given in Fig. 5. For the four values of θ_2

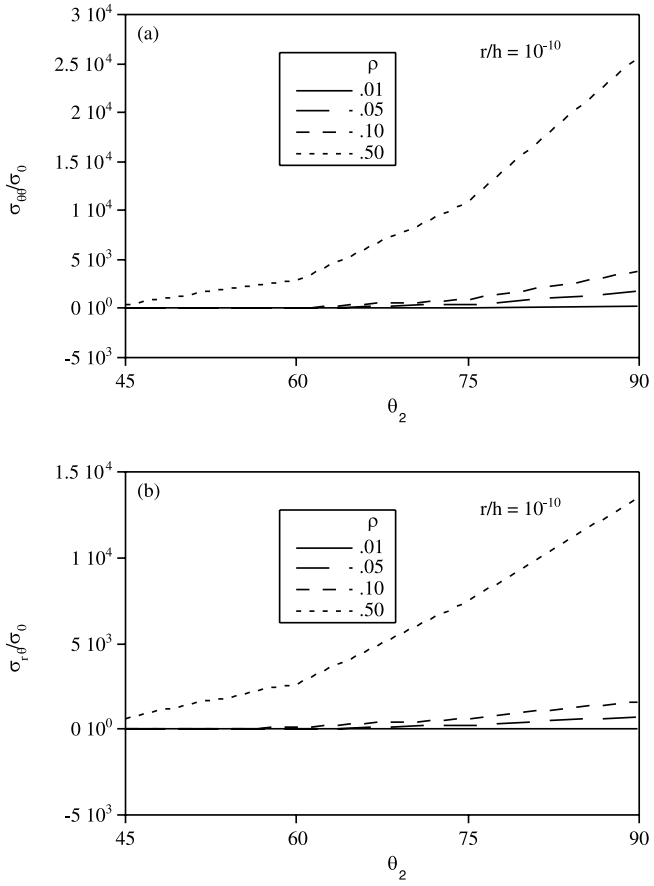

Fig. 9. (a) Normal and (b) shear stresses at corner A.

considered here, the stress singularity changes in an irregular fashion. The corresponding stress intensity factors are plotted in Fig. 12(a) and (b). The stress intensity factors increase with increasing ρ. However it can be seen that the stresses and stress intensity factors are not in direct correspondence. Hence, in contrast to the crack problem, stress intensity factors for different corners cannot be used by themselves to indicate the severity of the corners.

The same type of analysis was carried out for the joint shown in Fig. 3(a). The stress singularity values at corner C are plotted in Fig. 13. As expected, the singularity disappears for $\theta_2 = 180°$ as the joint C becomes a straight edge. The singularity decreases for increasing stiffness ratio, ρ and does not have a complex component. There is another bimaterial corner D in this structure and its singularities are plotted in Fig. 14. Again, as in the case of corner A in Fig. 4, there is a local minimum in the singularity value where the imaginary component originates. The singularity disappears for $\theta_1 > 135°$.

Considering only the stress singularities as plotted in Figs. 13 and 14, the lowest singularity for the structure in Fig. 3(a) occurs at two angles. One of them is when $\theta_2 = 180°$ $(\theta_1 = 90°)$. This corresponds to a butt joint and the corner C disappears. In that case, only the singularity at the corner D has to be accounted for. Another combination of angles is $\theta_2 = 270°$ and $(\theta_1 = 135°)$, approximately. The singularity at corner D disappears (Fig. 14) and only the singularity at the corner C has to be accounted for (Fig. 13).

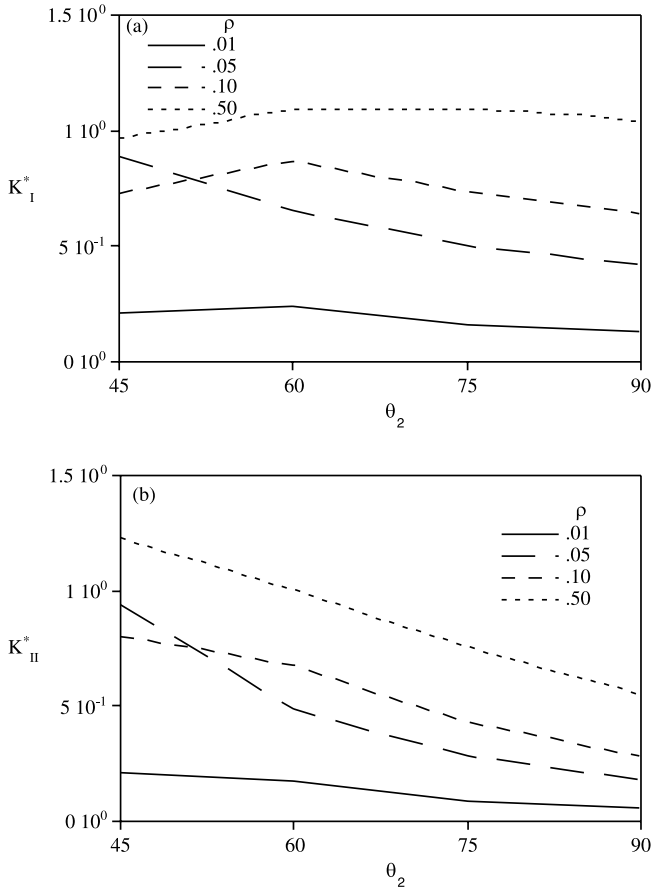

Fig. 10. Stress intensity factors for corner A.

The stress intensity factors were found for two different angles. The intensity factors along with the stress values were obtained using the RWCIM for the outermost contour, C4 in Fig. 3(c) and are given in Tables 1 and 2. Again, it was noted that as the angle changes (and the dominant singularity), the stress intensity factors and the stresses were not in correspondence. This means that the stress intensity factors by themselves cannot be used to represent the severity of the corner.

3.2. J_2 deformation plasticity solution

For J_2 deformation analysis, material 1 was assumed to be rigid and material 2 was taken to be J_2 deformation plastic with $v_2 = 0.5$ (incompressible). The fourth order differential equation (Eq. (15)) with the boundary conditions (Eq. (14)) was solved for the eigenvalues λ. The multiple shooting method with the Runge–Kutta scheme was used to integrate the differential equation. For verification purposes, it was confirmed that for $n = 1$, the singular values found by this method matched the ones found by the elastic analysis for $v_2 = 0.5$ and ρ tending to zero. In addition, the singular values for the $\theta_2 = 90°$ matched exactly with the ones given by Reedy (1993).

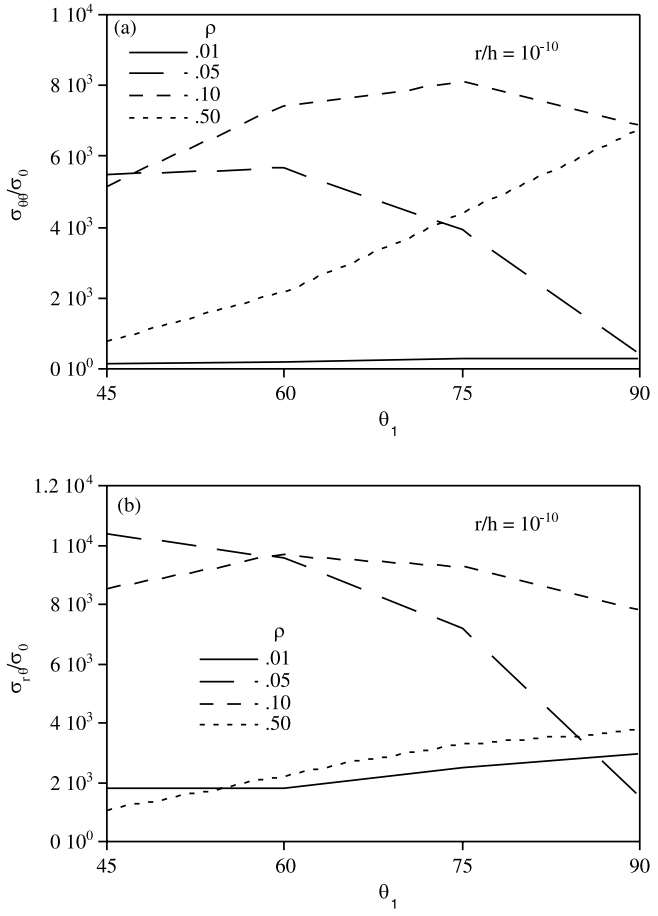

Fig. 11. (a) Normal and (b) shear stresses at corner B.

The stress singularity for the corner A shown in Fig. 2(a) is plotted in Fig. 15. As expected, the singularity decreases with increasing hardening exponent and increases with increasing θ_2. For low values of the hardening exponent, there is a marked change in the value of the singularity with θ_2. For $n = 1$, the singularity rises sharply from $\lambda = 0.087$ for $\theta_2 = 50°$ to $\lambda = 0.405$ for $\theta_2 = 90°$. The increase is much smaller from $\theta_2 = 90°$ to $\theta_2 = 180°$, where $\lambda = 0.5$. In what follows, since the sensitivity was very high for $\theta_2 < 90°$, the stress intensity factors were only found for $\theta_2 = 60°$, 75°, and 90°.

The non-dimensionalized stress intensity factors for the J_2 deformation plasticity analysis are defined as

$$K_{\mathrm{I}}^{\mathrm{p}} = \left(\frac{r}{h}\right)^{\lambda} \frac{\sigma_{\theta\theta}(\theta = 0)}{\sigma_0}$$

and

$$K_{\mathrm{II}}^{\mathrm{p}} = \left(\frac{r}{h}\right)^{\lambda} \frac{\sigma_{r\theta}(\theta = 0)}{\sigma_0} \tag{19}$$

where h is the thickness of the specimen and σ_0 is the applied stress.

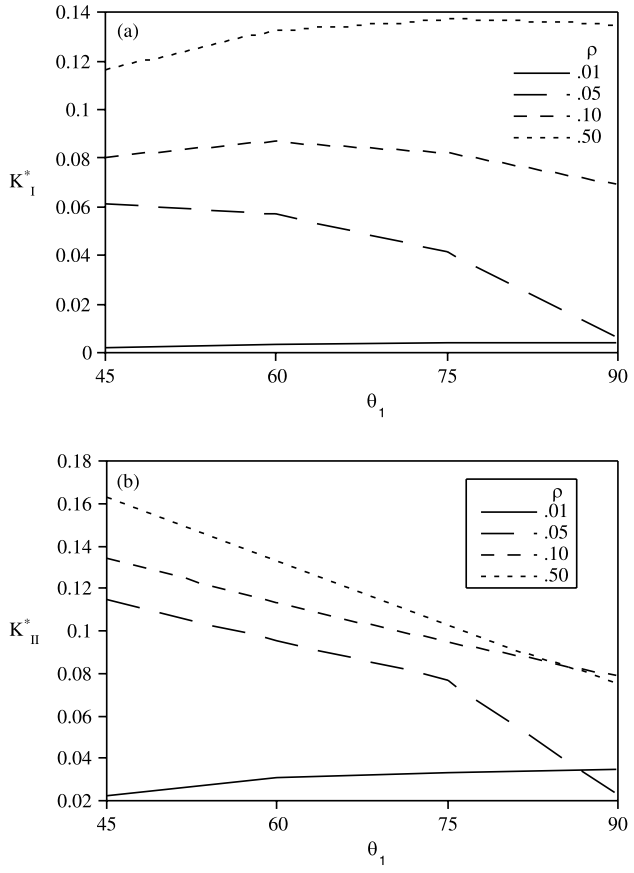

Fig. 12. Stress intensity factors for corner B.

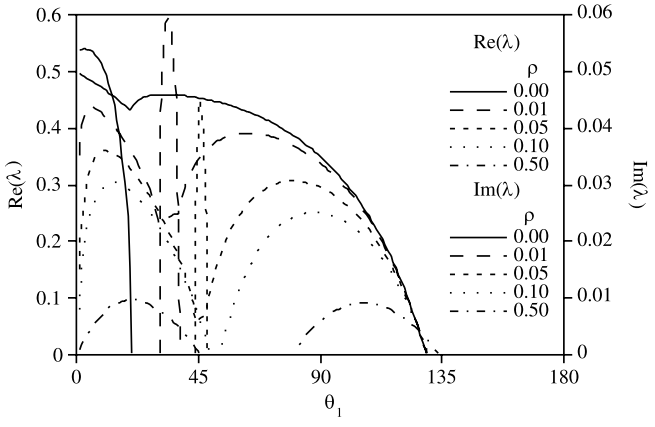

Fig. 13. Stress singularity at corner C in Fig. 3(a).

The stress intensity factors were found from finite element solutions obtained with a very fine mesh near the corner. The material constants used were $E_2 = 1.55$ GPa, $\sigma_y = 0.137$ MPa, $\alpha = 0.07$, $n = 8$ and the

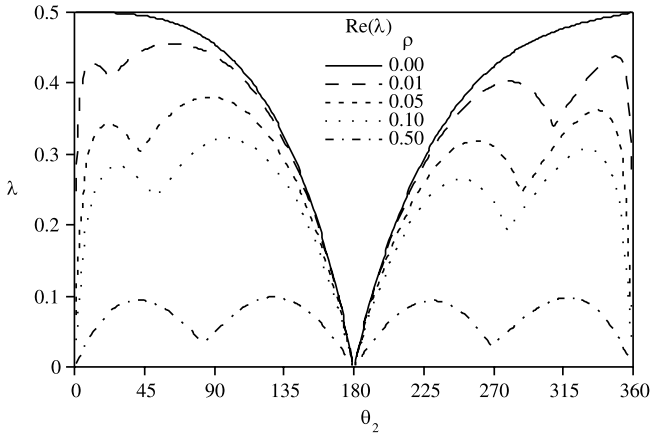

Fig. 14. Stress singularity at corner D in Fig. 3(a).

Table 1
Stresses and stress intensity factors for corner C ($\theta_2 = 270°$)

ρ	λ	$\sigma_{\theta\theta}/\sigma_0$	K_I	$\sigma_{r\theta}/\sigma_0$	K_{II}
0.01	0.3971	−7283.1	−0.7791	−4415.5	−0.4723
0.05	0.3106	24405.1	19.13	11941.1	9.358
0.10	0.2319	11.890	0.05704	4.6644	0.02238
0.50	0.03338	0.97685	0.4529	−0.20429	−0.09472

Table 2
Stresses and stress intensity factors for corner ($\theta_2 = 90°$)

ρ	λ	$\sigma_{\theta\theta}/\sigma_0$	K_I	$\sigma_{r\theta}/\sigma_0$	K_{II}
0.01	0.4391	2656.6	0.1081	−1955.48	−0.07955
0.05	0.3804	−757.27	−0.1189	526.888	0.08275
0.10	0.3195	362.41	0.2316	−235.157	−0.1503
0.50	0.04745	0.14734	0.04942	−0.03358	−0.01126

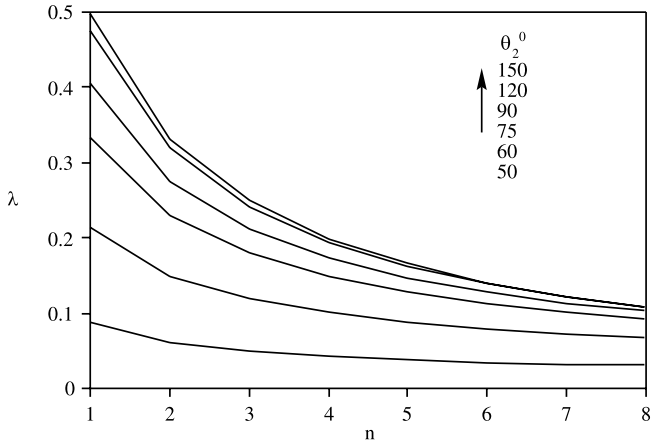

Fig. 15. The stress singularity at corner A using elastoplastic analysis.

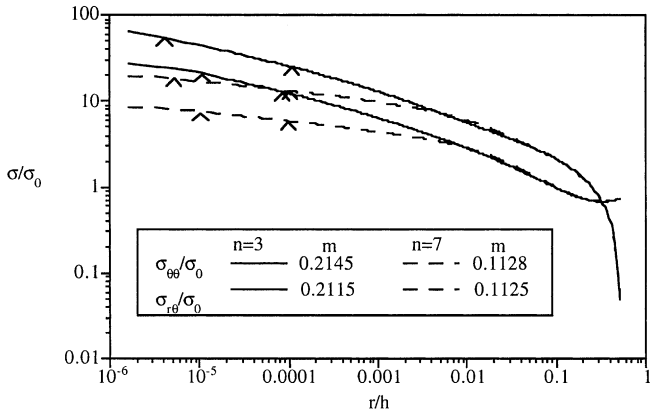

Fig. 16. Determination of stress intensity factors using FEM solution.

applied load was $\sigma_0 = \sigma_y/4$. A small value of yield stress was chosen to ensure that large plastic deformations occurred near the corner. As can be seen from Eq. (17), when a logarithmic plot is made of $\sigma_{\theta\theta}/\sigma_0$ vs. r/h or $\sigma_{r\theta}/\sigma_0$ vs. r/h, the intercepts are $\log(K_I^p)$ and $\log(K_{II}^p)$ respectively.

A plot of these curves is shown in Fig. 16 where the corner with $\theta_2 = 90°$ was considered with $n = 3$ and 7. The regions over which the slope (m) is within 1% of the λ values found using the differential equation are also shown. This provides additional verification of the singularity values obtained from the differential equation. This also shows that there is indeed a zone around the corner that is dominated by the plastic stress singularity.

The plot was made for stress values up to $r/h = 0.5$. The stress values for $r/h > 0.5$ were not plotted as they were negative and hence cannot be plotted in a logarithmic plot. This shows that the boundary effects are dominant for $r/h > 0.5$. In fact, the boundary effects can even be seen for $r/h > 0.1$ in Fig. 16. The zone over which the plastic singularity dominates lies in between $10^{-6} < r/h < 10^{-4}$. There does not seem to be a region where linear elastic singularity dominates as the curves do not have a slope corresponding to the elastic singularity value before the boundary effects dominate. For the elastic analysis results shown in Fig. 7(a) and (b), the dominant zone for the elastic singularities was found to be $r/h < 10^{-5}$. Hence, this region is taken over by the plastic singularity zone for the low yield strength that was considered here.

The plastic stress intensity factors are given in Fig. 17. The K_{II}^p is nearly constant for the ranges of angles and hardening exponents considered but K_I^p increases both with respect to the angle and the hardening exponent. This is consistent with the results of an experimental study with a somewhat different geometry (Mohammed and Liechti, 2000), where it was found that crack nucleation loads increased with decreasing corner angle.

For a lap joint as shown in Fig. 2(a), the applied stress is expected to yield a high shear stress along the interface. This was the case as it was found from the finite element solution that $\varepsilon_{\theta\theta} = 0.56\%$ and $\gamma_{r\theta} = 8.2\%$ at $r/h = 10^{-6}$. For a fully plastic material, Reedy (1993) has shown that, based on Ilyushin's theorem, the stress intensity factor depends only on the hardening exponent. He did not study the effect of varying angle. As the loading arrangement here is such that the whole region is not plastic, his result may not apply here. For this lap joint with fixed load, the normal strain is much smaller than the shear strain. It can be seen from Fig. 17 that K_I^p increases with the corner angle and hardening exponent whereas K_{II}^p remains constant. The fact that there is a strong dependence on the angle when the strain is small (K_I^p) and very little when the strain is high (K_{II}^p) indicates the dependence of non-dimensionalized stress intensity factor on a load-like parameter and the corner singularity, λ.

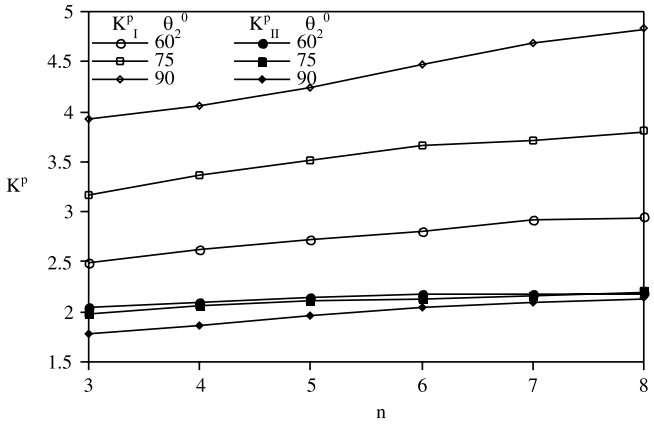

Fig. 17. Stress intensity factors for corner A using elastoplastic analysis.

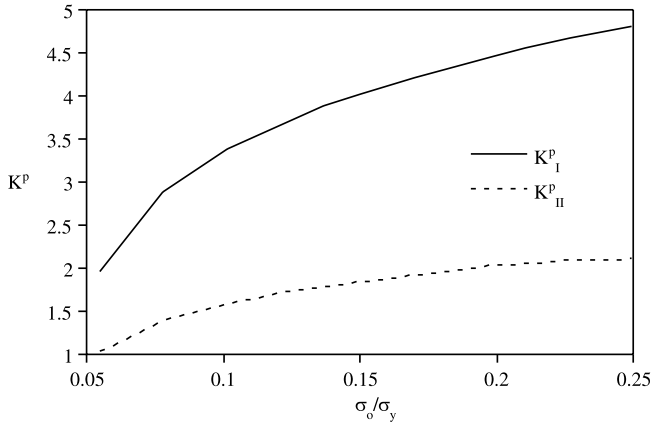

Fig. 18. Applied load dependence on the stress intensity factors.

To study the effect of the variation of load, the stress intensity factor is plotted for increasing applied load in Fig. 18. This figure is plotted for $n = 8$ and $\theta_2 = 90°$. The non-dimensionalized stress intensity factor does indeed show dependence on the magnitude of the load though its rate of increase does decay with load. The same analysis was attempted for the corner C in Fig. 3(a) but the stress values and the stress intensity factors were found to be very small. For the same load, due to high constraints, there is a large hydrostatic stress and very small shear stress, giving rise to small values of stress intensity factors along the interface.

4. Conclusions

The aim of this work was to study the severity of bimaterial corners with respect to the angle and investigate the appropriateness of using stress intensity factors as measure of severity of a bimaterial corner with arbitrary angle. A variety of bimaterial corners with different material properties and corner angles were analyzed. In the elastic analysis, both the materials were taken as linear elastic materials and the ratio of the stiffness was varied. The main conclusions are:

- The dominant stress singularity, λ_1, generally increases with decreasing corner angle except for a slight decrease where the singularity has a complex component.
- The range of the dominant singularity is $0 < \mathrm{Re}(\lambda) < 0.5$. Depending on the corner angle and the stiffness ratio, there may be more than one singularity and there are an infinite number of non-singular eigenvalues.
- In the lap joint problem, the stress singularity when the stiffer material angle is varied (corner B) is more severe than when the more complaint material angle is varied (corner A).
- More than one singular eigenvalue (if it exists) is needed to increase the range over which the eigenvalue solutions (stresses and displacements) are valid.
- By comparing the stresses and stress intensity factors for corner A and B, it was found that the stress intensity factors by themselves cannot characterize the corner.
- The stress singularity for a joint (both sides bonded) did not exhibit a complex component for a wide range of stiffness ratios and corner angles.
- The lack of correspondence in stresses and stress intensity factors was also found in the case of a scarf joint. It was concluded that the variation of stress intensity factors with the corner angles and stiffness ratios cannot be predicted and hence they cannot be used as a nucleation criterion.

J_2 deformation analysis was carried out by assuming one material to be rigid and the other one to be an incompressible elastoplastic material. A fourth order differential equation was obtained and solved to obtain the stress singularities. Finite element solutions with a very fine mesh were used to obtain the stress intensity factors. The main conclusions drawn from this analysis are:

- The stress singularity decreased with increasing hardening exponent and increasing corner angle.
- The normal plastic stress intensity factor ($K_{\mathrm{I}}^{\mathrm{p}}$) increased with decreasing corner angle and increasing hardening exponent. The shear plastic stress intensity factor ($K_{\mathrm{II}}^{\mathrm{p}}$) was relatively insensitive to both the parameters. This may be due to the high shear strain (8.2%) and small normal strain (0.56%) present near the corner ($r/h = 10^{-6}$ along the interface).
- The non-dimensionalized plastic stress intensity factors flattened out for large values of applied load. In this case (Fig. 17), close to corner, the stress component that has yielded gives rise to stress intensity factor that is independent of angle. This may be useful as a crack nucleation criterion when there is substantial yielding.

References

Bogy, D.B., 1971. Two edge-bonded elastic wedges of different materials and wedge angles under surface tractions. Journal of Applied Mechanics 38, 377–386.

Carpenter, W.C., Byers, C., 1987. A path independent integral for computing stress intensities for V-notched cracks in a bimaterial. International Journal of Fracture 35, 245–268.

Duva, J.M., 1988. The singularity at the apex of a rigid wedge embedded in a nonlinear material. Journal of Applied Mechanics 55, 361–364.

Fernlund, G., Papini, M., McCammond, D., Spelt, J.K., 1994. Fracture load predictions for adhesive joints. Composites Science and Technology 51, 587–600.

Gradin, P.A., 1982. A fracture criterion for edge-bonded bimaterial bodies. Journal of Composite Materials 16, 448–456.

Groth, H.L., Brottare, I., 1988. Evaluation of singular intensity factors in elastic–plastic materials. Journal of Testing and Evaluation 16, 291–297.

Hattori, T., Sakata, S., Murakami, G., 1989. A stress singularity parameter approach for evaluating the interface reliability for plastic encapsulated LSI devices. Journal of Electronic Packaging 111, 243–248.

Hein, V.L., Erdogan, F., 1971. Stress singularities in a two-material wedge. International Journal of Fracture Mechanics 7, 317–330.

Lau, C.W., Delale, F., 1988. Interfacial stress singularities at free edge of hybrid metal matrix composites. Journal of Engineering Materials and Technology 110, 41–47.

Mohammed, I., Liechti, K.M., 2000. Cohesive zone modeling of crack nucleation at bimaterial corners. Journal of the Mechanics and Physics of Solids 48, 735–764.

Muskhelishvili, N.I., 1963. Some basic problems of the mathematical theory of elasticity. Groningen P. Noordhoff Publications.

Reedy Jr., E.D., 1993. Free edge stress intensity factor for a bonded ductile layer subjected to shear. Journal of Applied Mechanics 60, 715–720.

Reedy Jr., E.D., Guess, T.R., 1993. Comparison of Butt tensile strength data with interface corner stress intensity factor prediction. International Journal of Solids and Structures 30, 2929–2936.

Stern, M., Becker, E.B., Dunham, R.S., 1976. A contour integral computation of mixed-mode stress intensity factors. International Journal of Fracture 12, 359–368.

Yang, Y.Y., Munz, D., 1995. Stress distribution in a dissimilar materials joint for complex singular eigenvalues under thermal loading. Journal of Thermal Stresses 18, 407–419.

Williams, M.L., 1952. Stress singularities resulting from various boundary conditions in angular corners of plates in extension. Journal of Applied Mechanics 74, 526–528.